Geophysical Journal International

# Source parameters of the 2008 Bukavu-Cyangugu earthquake estimated from InSAR and teleseismic data

| | |
|---|---|
| Journal: | *Geophysical Journal International* |
| Manuscript ID: | GJI-10-0252.R2 |
| Manuscript Type: | Research Paper |
| Date Submitted by the Author: | n/a |
| Complete List of Authors: | d'Oreye, Nicolas; National Museum of Natural History, Geophysics/Astrophysics; European Center for Geodynamics and Seismology<br>González, Pablo; Instituto de Astronomia y Geodesia (CSIC-UCM)<br>Shuler, Ashley; Columbia University, Lamont-Doherty Earth Observatory<br>Oth, Adrien; European Center for Geodynamics and Seismology<br>Bagalwa, Louis; Observatoire Volcanologique de Goma<br>Ekstrom, Goran; University of Colombia, LDEO<br>Kavotha, Sadaka; Observatoire Volcanologique de Goma<br>Kervyn, François; Royal Museum for Central Africa, Earth Sciences Department<br>Lucas, Célia; National Museum of Natural History, Geophysics/Astrophysics; European Center for Geodynamics and Seismology<br>Lukaya, François; Observatoire Volcanologique de Goma<br>Osodundu, Etoy; Observatoire Volcanologique de Goma<br>Wauthier, Christelle; Royal Museum for Central Africa, Earth Sciences Department; University of Liege, Dept. ArGEnCo<br>Fernández, Jose; Instituto de Astronomia y Geodesia (CSIC-UCM), Facultad de Ciencias Matematicas |
| Keywords: | Radar interferometry < GEODESY and GRAVITY, Earthquake source observations < SEISMOLOGY, Seismicity and tectonics < SEISMOLOGY, Body waves < SEISMOLOGY, Continental tectonics: extensional < TECTONOPHYSICS, Africa < GEOGRAPHIC LOCATION |
| | |

# Source parameters of the 2008 Bukavu-Cyangugu earthquake estimated from InSAR and teleseismic data

*Nicolas d'Oreye[1,4], Pablo J. González[2], Ashley Shuler[3], Adrien Oth[4], Louis Bagalwa[5], Göran Ekström[3], Déogratias Kavotha[5], François Kervyn[6], Celia Lucas[1,4], François Lukaya[5], Etoy Osodundu[5], Christelle Wauthier[6,7], José Fernández[2]*

[1]Dept. Geophys./Astrophys., National Museum of Natural History, 19 rue Josy Welter, 7256 Walferdange, Luxembourg, ndo@ecgs.lu

[2]Instituto de Astronomia y Geodesia (CSIC-UCM), Plaza de Ciencias 3, 28040-Madrid, Spain

[3]Lamont-Doherty Earth Observatory, Department of Earth and Environmental Sciences, Columbia University, NY, USA

[4]European Center for Geodynamics and Seismology, 19 rue Josy Welter, 7256 Walferdange, Luxembourg

[5]Goma Volcano Observatory, Democratic Republic of Congo

[6]Earth Sciences Department, Royal Museum for Central Africa, 3080 Tervuren, Belgium

[7]Dept. ArGEnCo, University of Liege, Sart Tilman B52, 4000 Liège, Belgium

Accepted *date*. Received *date*; in original form *date*

Abbreviated title: Source parameters of the 2008 Bukavu-Cyangugu earthquake

Corresponding author: Nicolas d'Oreye, Dept. Geophys./Astrophys., National Museum of Natural History, 19 rue Josy Welter, 7256 Walferdange, Luxembourg, ndo@ecgs.lu. Tel: +352 33 14 87 1. Fax: +352 33 14 87 88

**Keywords**

Radar interferometry; Earthquake source observations; Seismicity and tectonics; Body waves; Continental tectonics: extensional; Africa

**Abstract**

Earthquake source parameter determination is of great importance for hazard assessment, as well as for a variety of scientific studies concerning regional stress and strain release and volcano-tectonic interaction. This is especially true for poorly instrumented, densely populated regions such as encountered in Africa, where even the distribution of seismicity remains poorly documented. In this paper, we combine data from satellite radar interferometry (InSAR) and teleseismic waveforms to determine the source parameters of the $M_w$ 5.9 earthquake that occurred on 3 February 2008 near the cities of Bukavu (DR Congo) and Cyangugu (Rwanda). This was the second largest earthquake ever to be recorded in the Kivu basin, a section of the western branch of the East African Rift (EAR). This earthquake is of particular interest due to its shallow depth and proximity to active volcanoes and Lake Kivu, which contains high concentrations of dissolved carbon dioxide and methane. The shallow depth and possible similarity with dyking events recognized in other parts of EAR suggested the potential association of the earthquake with a magmatic intrusion, emphasizing the necessity of accurate source parameter determination. In general, we find that estimates of fault plane geometry, depth, and scalar moment are highly consistent between teleseismic and InSAR studies. Centroid-moment-tensor (CMT) solutions locate the earthquake near the southern part of Lake Kivu, while InSAR studies place it under the lake itself. CMT solutions characterize the event as a nearly pure double-couple, normal faulting earthquake occurring on a fault plane striking 350° and dipping 52° east, with a rake of -101°. This is consistent with locally mapped faults, as well as InSAR data, which place the earthquake on a fault striking 355° and dipping 55° east, with a rake of -98°. The depth of the earthquake was constrained by a joint analysis of teleseismic P and SH waves and the CMT data set,

showing that the earthquake occurred in the shallow crust, at approximately 8 km depth. Inversions of ENVISAT and ALOS data place the earthquake at 9 km. A comparison of the scalar moment ($9.43 \pm 0.06 \times 10^{17}$ Nm from seismology and $8.99 \pm 0.010 \times 10^{17}$ Nm from the joint InSAR solution) shows good agreement between the two datasets. Such an agreement is in contrast to the large discrepancies observed (up to an order of magnitude) in other places along the EAR where similar earthquake sequences are associated with magmatic intrusion. From this, we infer that the rupture was brittle and occurred with little aseismic deformation as might be expected from magma injection. Our results provide insights into the style of rifting occurring in the South Kivu Volcanic Province and hence will aid future studies on seismic risk in the context of Lake Kivu and underline the importance of systematic monitoring of the EAR area.

## 1. Introduction

On 3 February 2008 at 07:34:12 UTC (09:34 local time), a $M_w$ 5.9 earthquake occurred near the cities of Bukavu and Cyangugu, along the border between South Kivu Province of the Democratic Republic of Congo and the Rusizi District in the West Province of Rwanda (Figure 1). This earthquake (Bukavu-Cyangugu, or more simply the Bukavu earthquake) was followed by many felt aftershocks, ten of which were large enough to be recorded in the USGS earthquake catalog. Additionally, a temporary local seismic network composed of three stations installed by Goma Volcano Observatory on February 8th recorded more than 700 aftershocks over the following three weeks.

This series of earthquakes caused widespread damage in DR Congo and Rwanda, with the mainshock being felt as far away as Nairobi, Kenya, 850 kilometers away. According to local authorities, at least 37 people were killed in Rwanda and 7 more in DR Congo. The United Nations Office for the Coordination of Humanitarian Affairs (OCHA) reported 1090 injured and nearly 5000 buildings damaged in DR Congo and Rwanda (OCHA 2008).

The Bukavu earthquake was devastating to the region, in part because of its magnitude, but also due to its shallow depth. To aid future studies on seismic risk in this densely populated, seismically active region, we work towards relocating the hypocenter of this earthquake, and determining its scalar moment and faulting mechanism using two independent data sets – teleseismic waveforms and InSAR data. For large earthquakes, satellite radar interferometry (InSAR) (Massonnet & Fiegl 1998) has proved to be an important, complementary tool for source parameter estimation. Though InSAR inversions are unable to differentiate ground deformation resulting from distinct events closely spaced in time (i.e., between satellite acquisitions), they do not suffer from systematic errors caused by inadequate station coverage. In addition, they are much less dependent on velocity models than teleseismic source studies (Mellors et al. 2004). The largest sources of error associated with inverting InSAR data for source parameters are due to vegetation-induced decorrelation and atmospheric artifacts. For moderate-sized earthquakes, InSAR has been only occasionally successful in determining source parameters of shallow events occurring in arid or semi-arid areas (Rigo & Massonnet 1999; Stramondo et al. 1999; Kontoes et al. 2000; Lohman et al. 2002; Amelung & Bell 2003; Dawson et al 2008; Feigl & Thurber 2009). Fortunately, in this case, although the Bukavu earthquake occurred in a vegetated, high-relief area, the coseismic deformation was captured successfully by both the ENVISAT ASAR and the ALOS PALSAR radar sensors, allowing the construction of two independent interferograms with favorable temporal and spatial baselines.

In this paper, we describe the source model resulting from the inversion of teleseismic waveforms from the Global Seismographic Network. We use this information, along with inversions from the ENVISAT and ALOS interferograms, to locate the hypocenter accurately, as well as to constrain source parameters such as scalar moment and the strike and dip of the ruptured fault. We discuss the agreement between the results of these two independent methods with observations from local field investigations and partial relocation of aftershocks. Finally, we present our results in the context of the seismic and tectonic history of the region.

## 2. Regional Setting

The East African Rift (EAR) extends over 6000 kilometers from the Afar Triple Junction in Ethiopia to offshore Mozambique, forming the divergent boundary between the Nubian and Somalian plates (Foster & Jackson 1998; Stamps et al. 2008). The EAR divides into two branches surrounding the mechanically strong Tanzanian craton. Unlike the Eastern branch, the Western Rift experiences intense seismicity and moderate volcanism.

The Western Rift is formed by the succession of 40-70 kilometer-wide basins characterized by grabens and half-grabens in 100 kilometer-long segments (Ebinger 1989; Ebinger et al. 1991). It is here that the deep and anoxic African Great Lakes are nested. Successive basins are linked by accommodation zones characterized by oblique-slip transfer faults and volcanic provinces such as the Virunga (Ebinger et al. 1989).

The Bukavu earthquake occurred near the southern shore of Lake Kivu, roughly 100 km south of the city of Goma (DR Congo) and the active volcanoes of the Virunga chain, Nyiragongo and Nyamulagira (Figure 1). While the Virunga volcanic province has been active since the mid-Miocene, the South Kivu volcanic province is considered extinct, despite evidence of Upper Cenozoic volcanism (Ebinger et al. 1991). The Bukavu seismic sequence occurred at the southern end of the asymmetric West Kivu basin. Border faults of that rift segment are sub-vertical normal faults trending mostly North-South (Villeneuve 1980; Delvaux & Barth 2010). The high throws (2 to 5 kilometers) and the dips ranging from 40° to 70° are inferred from earthquake focal mechanisms (Ebinger 1989; Morley 1989). They are approximately planar, like the majority of faults in the EAR, and are believed to maintain their steep dips to depths of 7 km or more (Morley 1989; Ebinger et al. 1991). The rate of extension in this region of the EAR is estimated at 2.8 mm/yr, and the average effective elastic plate thickness is constrained to be 21-36 km (Stamps et al. 2008; Tessema & Antoine 2003), significantly less than the largely unfaulted Tanzanian craton (>70 km) (Pérez-Gussinyé et al. 2009).

## 3. Background Seismicity

Earthquakes larger than magnitude 5 are uncommon in the Kivu basin (Mavonga 2007; Barth et al. 2007; Mavonga & Durrheim 2009; Delvaux & Barth 2010). According to the USGS catalog (1973 to present), the Bukavu earthquake is the second largest earthquake recorded in this area, following the $M_w$ 6.2 earthquake that occurred on 24 October 2002 in the northern part of Lake Kivu (Figure 2). Besides aftershocks from those two largest events, swarms of moderate-sized earthquakes also occurred in 1977 and 2002, coincident with the only two recorded fissure eruptions of Nyiragongo volcano. Indeed, the activity of Nyiragongo and Nyamulagira is believed to be directly related to the opening of the Western Rift Valley (Kasahara et al. 1992; Wauthier et al., in prep.). The 2002 eruption of Nyiragongo, for example, occurred during a regional rifting event between the volcano and Lake Kivu (Komorowski et al. 2002/2003; Tedesco et al. 2007). In addition, the 1977 eruption of Nyiragongo occurred four days after a $M_w$ 5.3 event struck the Bukavu area (Hamaguchi et al. 1992). Despite the temporal link between several moderate earthquakes and volcanic activity, it should be noted that minor to moderate earthquakes occur frequently in this region, and many of these are not linked to eruptions. This is true both for the Bukavu earthquake itself, as well as for two M>4 earthquakes that occurred in October 2008 approximately 50 km north of Goma, DRC.

## 4. Field Observations

Only two days after the Bukavu earthquake, a team of geologists led by one of the authors investigated the epicentral area where many damaged buildings were reported (F. Kervyn, pers. com.). Although an extensive search for fault scarps was conducted, the only visible traces of the earthquake were numerous ground cracks and small landslides. Extensive damage occurred on the Birava peninsula area, near the epicenter location provided by the USGS (Figure 1). In the village of Birava, the back wall of an old church was damaged and the bell-tower of a recently erected church sank a few centimeters into the ground. Fallen unreinforced masonry walls and sheared pillars were observed at the village school. Observations were also conducted offshore, on the island of Ibinja, where casualties were reported. An underwater landslide caused a 30-50-meters-wide manioc crop field at the shoreline to slide about 10 meters into the lake, causing a local tsunami that swept two villagers away. Only the upper parts of submerged banana trees were still visible (Figure 3). Interestingly, geomorphologic evidence in the southern part of the island suggests that landslides have occurred frequently in this area.

## 5. Seismology

### 5.1. Local Seismic Data

The Bukavu earthquake was followed by several moderate-sized aftershocks. Eleven earthquakes, ranging in magnitude from 3.7-5.9, were recorded in the USGS catalog. In addition, over 700 aftershocks were recorded by a local seismic network, which was installed on 8 February 2008 and operated for three weeks.

This temporary network consisted of six analog seismometers equipped with drum recorders, - three stations installed in the epicentral area at Bukavu (BKV), Birava (BRV) and Kabare (KAB), and three at Lwiro (LWI), Luboga (LBG) and Rusayo (RSY). These analog stations complemented the permanent digital seismic network of Goma Volcano Observatory (GVO), which contains six short-period 1Hz Kinematics seismometers installed at Rusayo (RSY), Bulengo (BLG), Kibumba (KBB), Kibati (KBT), Katale (KTL) and Goma (OVG) (Figure 4). Unfortunately, the GVO local seismic network was not operational during the mainshock, but was brought online after the event.

The local seismic network was able to record a fraction of the aftershocks, but several factors must be taken into account when interpreting the event locations. First, the majority of aftershocks went unrecorded by the local network. Without the first five days of measurements, and based on the rate of decay of the aftershock series observed over three weeks, we conservatively estimate using the Modified Omori's law (Utsu 1961) that only 20-40% of the aftershocks were recorded by the local network. In addition, out of the 700 earthquakes recorded by the local network, only 68 were recorded by at least four stations, allowing relocation using Nonlinloc software (Lomax et al. 2000). These events represent 1-4% of the total aftershocks sequence.

In addition to these shortcomings, there are several sources of error in the aftershock locations. First, the unfavorable geographic distribution of the seismic stations most likely results in a bias in the earthquake locations. All the stations of the temporary network are located west of the epicenter of the mainshock, and the GVO permanent stations are all located at similar distances and in a narrow azimuthal range to the north. Second, the location errors may be underestimated because the calculation of hypocenter location uncertainty assumes a normal distribution of the errors, a condition that is not met by the available 4-6 phase measurements. Finally, in the absence of a detailed local velocity model, we use a simple 1-D model derived from velocity structure investigations by Bonjer et al. (1970) and Bram (1975) (Table 1).

The results of local seismic observations show a clustering of epicenters in a 40x20-km-wide zone south of Lake Kivu (Figure 4). This area is too large to be associated with an identified fault or specific geologic structure. In addition to the plausible epicentral location bias, it is not clear whether the aftershocks recorded a few days after the mainshock are related to slip on the same fault, or to reactivation of one of the numerous nearby faults. Likewise, it is difficult to determine the depths of the earthquakes. The aftershocks cluster at shallow depths of a few kilometers, and in a deeper zone around 15 km depth, though these depths are strongly dependent on the velocity model. Performing the same calculation using slightly different velocity models showed dramatic differences in the estimated clustering depths. In addition, the effect of the steep and highly faulted topography (500 m deep lake surrounded by 2-5 km high escarpments) is not modeled, and may be significant.

### 5.2. Centroid-Moment-Tensor Solutions

In the absence of an operational local seismic network during the mainshock, we use data from the Global Seismographic Network to determine the focal mechanism, depth, and scalar moment of the Bukavu earthquake. Our inversion is supplemented by additional data from the SEARIFT and Afar Consortium seismic arrays in Ethiopia (Ebinger et al. 2010). Centroid-moment-tensor (CMT) solutions were calculated following the methods of Dziewonski et al. (1981) and Arvidsson and Ekström (1998). In these methods, the moment tensor and source centroid are estimated by matching observed three-component seismograms to synthetic waveforms calculated by a summation of normal modes. Both body and surface waves were used in the inversion, and care was taken to ensure that solutions were based on waveforms from a variety of azimuths and distances.

The moment tensor resulting from the CMT analysis shows a nearly pure double-couple, normal-faulting earthquake with a scalar moment of $9.43 \pm 0.06 \times 10^{17}$ Nm.

The motion on one of the best-fitting nodal planes is described by the following angles: strike 350°, dip 52°, and rake -101° (Table 3). The data are best fit by a shallow depth for the source centroid, and the final solution was calculated for a fixed depth of 12 kilometers, the shallowest depth normally used in the CMT analysis.

CMT solutions were also calculated for two of the largest aftershocks ($M_w$ 5.0 on 3 February 2008 10:56:10 and $M_w$ 5.3 on 14 February 2:07:47), which similarly were found to have normal-faulting focal mechanisms and shallow focal depths (Figure 5). The centroids of these three earthquakes are located a few kilometers away from the cluster of seismicity recorded by the local network. However, their locations are not inconsistent with a mainshock epicenter there considering typical uncertainties in the estimate of the long-period centroid (Smith and Ekström, 1996).

### 5.3. Broadband Seismic Analysis

To constrain the focal depth of the earthquake, we performed a joint inversion of broadband teleseismic P and SH waveforms and the CMT data set using the methods of Ekström (1989). In the analysis, teleseismic broadband waveforms are used in an inversion for focal mechanism, focal depth, and source time function. The CMT estimate of the point source moment tensor is included as *a priori* information in the inversion to ensure that source models calculated from the broadband data are compatible with the long-period data used in the CMT analysis.

We begin by filtering each waveform to broadband displacement pulses (1-100 seconds period) by direct deconvolution of the instrument transfer function. SH waveforms are obtained by rotating the filtered horizontal records to the transverse direction. Synthetic P and SH seismograms are calculated using ray theory and the

281 Preliminary Reference Earth Model (PREM; Dziewonski & Anderson 1981).
282 Reflections and conversions near the source are included in the calculation by using a
283 layer matrix method for a regional velocity model. Again, we use the velocity model
284 derived from velocity structure investigations by Bonjer et al. (1970) and Bram
285 (1975), which was used to locate earthquakes in this region (Kavotha et al.
286 2002/2003; Mavonga et al. 2006; Mavonga 2007; Table 1).
287 The results from the best fitting source model can be seen in Figure 6. Overall, there
288 is excellent agreement between observed and synthetic P waveforms. The SH
289 waveforms show less agreement as is typical, but the main features of the SH
290 waveforms are modeled adequately. The best fitting broadband source model has a
291 focal mechanism that is very similar to the CMT solution and a centroid depth of 8 $\pm$
292 2 km. Thus, from our seismological data analysis, we conclude that the Bukavu
293 earthquake is a normal faulting earthquake, with a source in the shallow crust.
294
295
296 **6. Geodesy**
297 **6.1. Satellite Radar Interferometry (InSAR):**
298 Interferometric synthetic aperture radar (InSAR) has been used successfully to
299 measure ground deformation with a tens-of-meters spatial resolution and accuracy of
300 centimeters to sub-centimeters over broad areas, typically in satellite images
301 measuring 100 by 100 square kilometers (Massonnet & Fiegl 1998). The resolution in
302 the line of sight (LOS) direction depends on the radar wavelength. The European
303 Space Agency (ESA) ENVISAT satellite is equipped with a C-band ASAR sensor
304 with a wavelength of 5.6 centimeters. The Japanese Space Agency (JAXA) ALOS
305 satellite uses a 23.6-centimeter wavelength L-band PALSAR sensor. One color cycle

(or fringe) depicted on an interferogram represents a phase delay of half the wavelength. This represents a possible ground displacement of 2.8 cm (ENVISAT) or 11.8 cm (ALOS) in the LOS.

For large earthquakes, InSAR has proved to be an important tool for source parameter estimation (Bürgmann et al. 2000; Dawson & Tregoning 2007; Pritchard & Fielding 2008; Biggs et al. 2009a and references therein). This method is independent of the seismic inversion, and does not suffer from uncertainties associated with inadequate station coverage and is relatively independent of velocity models (Mellors et al. 2004). However, InSAR cannot differentiate between distinct episodes of ground deformation that occur close together in space or between satellite acquisitions.

When the coseismic ground deformation is small, as in the case of moderate sized earthquakes, InSAR can only be used under favorable conditions, such as if the earthquake is shallow or occurs in an arid or semi-arid area. Lohman and Simons (2005), studying thrust earthquakes of magnitude $4.5>M_w>5.5$ in Iran, concluded that, in principle, it would be possible to detect earthquakes of magnitudes 4 and 5 if they are shallower than 5 and 15 km respectively. In practice, however, InSAR proves only occasionally useful for the study of $M_w < 6.0$ earthquakes (Rigo & Massonnet 1999; Stramonto et al. 1999; Kontoes et al. 2000; Lohman et al. 2002; Amelung & Bell 2003; Dawson et al. 2008; Feigl & Thurber 2009). Mellors et al. (2004) performed a study of four moderate-sized, shallow strike-slip and thrust earthquakes in southern California, where the seismic station coverage is among the best in the world, and found that the InSAR-derived estimate of hypocenter depth was “good and better than the seismic constraints in some cases”, concluding that InSAR can provide reliable source parameters of shallow, moderate-sized earthquakes in areas that lack dense seismic networks.

Fortunately for our analysis, Bukavu is located south of the Virunga volcanic chain, which has been systematically monitored by satellite radar interferometry since 2005 (d'Oreye et al. 2008). The rich ENVISAT database allowed us to compute an interferogram with baseline conditions favorable enough to overcome the dramatic vegetation-induced decorrelation (Table 2). The January 10 – February 14, 2008 ENVISAT interferogram shows a single deformation pattern with a peak-to-trough LOS deformation of about 10 centimeters (Figure 7d). Independently, a pair of ALOS PALSAR L-band images spanning December 29, 2007 – March 30, 2008 allowed the computation of a second interferogram that shows a similar pattern (Figure 7a). As the patterns of deformations are consistent (given the difference of looking angle) between the two interferograms which were calculated using images recorded by different sensors on different dates, we rule out the possibility that the observed deformation is strongly affected by atmospheric artifacts.

The ENVISAT interferogram was computed using the open-source Doris software from the Delft University of Technology (Kampes et al. 2003), and the ALOS interferogram with the ROI_PAC software (Rosen et al. 2004). We used the NASA Shuttle Radar Topography Mission (SRTM) digital elevation models provided by the USGS to remove the topographic phase (Farr et al. 2007). SNAPHU software was used for phase unwrapping (Chen & Zebker 2001).

Given the rather simple morphology of the deformation mapped by InSAR, the data were subsampled homogeneously to a resolution of 150 meters. Only areas with coherence above 0.2 were considered during the source inversion (Figure 7)

### 6.2. Modeling and inversion

The fault plane geometry was modeled using a rectangular dislocation with uniform slip embedded in a homogeneous, isotropic, elastic half-space (Okada 1985). Nine parameters are solved for in the inversion: the depth, the latitude and longitude of the top of the fault plane, the amount of dip- and strike-slip along the fault, the dip and strike angles, and the width and length of the dislocation.

The deformation map was inverted using an unconstrained direct search, nonlinear optimization algorithm based on the downhill simplex method of Nelder and Mead (1965). This method has the advantage of converging relatively quickly to a solution that minimizes the squared misfit between the observed and predicted LOS deformation. However, it is not a global optimization method. For this reason, we randomly choose the starting parameters within broad bounds to generate 100 uniformly distributed samples.

For each of the nine parameters in the inversion, the histogram of the set of best-fit solution parameters is approximated by a Gaussian from which we select the mean value as the optimal solution and estimate the standard deviation. Figure 8 shows the distributions of the solution parameters, which appear normal.

Inversions were computed for each ENVISAT and ALOS data set alone, as well as a combined inversion. To account for the different uncertainties in InSAR data due to the wavelength difference between L- and C-band, we also performed a weighted joint inversion minimizing the misfit function

$$\varepsilon = R^t\, W\, R$$

where $R = (d - m)$ is the residual vector, $W$ is the weighting matrix ($W = Q_{dd}^{-1}$), $d$ is the observation vector formed as $d=[d^{L\text{-band}}_1, \ldots, d^{L\text{-band}}_k, d^{C\text{-band}}_1, \ldots d^{C\text{-band}}_n]$, and $m$ is the simulated ground displacements for a given set of model parameters corresponding to the location and incidence (track azimuth) angle of the data points of d. It is reasonable to consider that errors in the data affect independently and equally all pixels within the interferograms. We hence consider the covariance matrix as diagonal ($Q_{dd} = \sigma\, \Sigma_{dd}$), where $\sigma$ has been assumed for L-band and C-band as one-sixth of the corresponding radar wavelength (i.e. one-third of an interferometric fringe). The weighted and non-weighted inversions lead to very similar results although the weighted inversion slightly lowers the estimated scalar moment.

Results of the inversions are shown in Table 3 and Figures 7-9. All the inversions of the geodetic data sets place the epicenter in the southern part of Lake Kivu, a few kilometers away from the centroid location determined by CMT analysis. The earthquake is estimated to have a centroid depth of approximately 9 kilometers (see Table 3 for the detailed results of the single and joint data sets inversions). The values of the strike, dip and rake for the best-fitting fault from the weighted joint inversion are 355°, 55° and -98° respectively, and are consistent with the results from the seismic inversion. The scalar moment estimated from the joint inversion ($8.99 \pm 0.004 \times 10^{17}$ Nm) differs less than 5% from for the scalar moment estimated by the seismic inversion.

A matrix plot of the 100 best fitting parameters (Figure 9) shows the correlation between each of the nine parameters. A linear trend in a scatter plot indicates a possible trade-off between two parameters. For instance, there is a linear trend between depth and the amount of dip-slip motion, so a deeper source would have to slip more to produce similar surface ground deformation. In the absence of additional data (e.g., InSAR data with a different look angle and geometry) it is not possible to constrain the source parameters further. However, the uncertainties and possible trade-offs remain low enough for an accurate source parameter assessment and the results are in good agreement with those obtained using seismic data. Moreover, the InSAR analysis provides us with the accurate epicenter location, which is the least resolvable parameter from our seismic study in the absence of local data.

## 7. Discussion:

### 7.1. The rupture plane.

Although seismic and geodetic inversions provide us with consistent results, both methods suffer from the same limitation in discriminating the rupture plane among the two nodal planes. In this paper, we have only described a rupture plane dipping roughly 60° east, however a rupture plane dipping to the west is also consistent with the data. Both seismic and geodetic inversions identified the second nodal plane as dipping respectively 39.7° or 30.° west, with a rake of -77° or -71° and striking to 186°.

Without additional data such as identified surface rupture or strong motion records, it is difficult to remove the ambiguity inherent to the double-couple source mechanism. Neither the mainshock nor its aftershocks can be attributed to a specific identified fault, and the area is characterized by numerous small grabens bordered with east- and westward dipping faults (Villeneuve 1980; Ebinger 1989) (Figure 1). Nonetheless, the East 60° dipping nodal plane is most likely the rupture plane since low angle ruptures are not usually favored in extending brittle layers (Morley 1989; Buck 1988 and references therein; Lerch et al. 2010). Also, geophysical and geological observations from the East African Rift usually depict high-angle border faults that maintain their dips to depths of 7 km or more (Ebinger et al. 1991 and references therein, Morley

2002). Rare occurrences of exposed low angles faults in the East Kivu basin are recognized as originally steep fault planes rotated to a shallower angle during shallow local slides. (Ebinger 1989).

### 7.2. Assessment of Potential Magma-Tectonic Interaction

Considering the large number of moderate-sized earthquakes occurring during the Bukavu sequence, it was reasonable to suspect the presence of magma-tectonic interaction. However, the seismic moment estimated from the CMT inversion differs by less than 5% from the geodetic moment estimated from InSAR. This is in contrast to the large (up to one order of magnitude) discrepancy observed e.g. in Northern Tanzania, Ethiopia, Saudi Arabia or Iceland. In these volcanic rift zones the observed geodetic signal that could not be explained by the seismicity was shown to be associated to magmatic dyke intrusion (Feigl et al. 2000; Wright et al. 2006; Pagli et al. 2007; Calais et al. 2008; Biggs et al. 2009b; Hamling et al. 2009; Keir et al. 2009; Ayele et al. 2009; Grandin et al. 2009; Baer et al. 2010; Palister et al. 2010, and references therein).

The present agreement suggests that the observed deformation is coseismic and related to a brittle rupture with almost no aseismic slip. We conclude that the Bukavu sequence did not involve magma movement, at least at shallow depth.

### 7.3 Impact of the homogeneous half space assumption.

Geodetic data were inverted assuming a rectangular dislocation embedded in a homogeneous half space. The impacts of these assumptions on source parameter estimation have been investigated for various sources of ground deformation such as tensile sources, slow slip, as well as thrust, strike-slip and normal faulting mechanisms (e.g. Bonaccorso et al. 2005; Montgomery-Brown et al. 2009; Cattin et al. 1999; Lohman et al. 2002; Masterlark & Hughes 2008; Dubois et al. 2008; Dawson et al. 2008).

For normal faulting dislocation, theoretical studies show that the homogeneous half space hypothesis compared to a multilayered medium might result in a depth underestimation of typically up to 10-15%. The slip might be overestimated of about 3-10%. On the other hand the dip angle would vary by less than 2 degrees (Cattin et al. 1999; He et al. 2003). These numbers can hence be considered as bounds to the accuracy of our inversion results.

Likewise, results from inversion of seismic data using a homogeneous velocity model similar to the homogeneous half space used for the inversion geodetic data do not change significantly the results. The focal mechanism and source time function look nearly identical to the solution obtained with the simple 1-D velocity model. Only the depth is <600 m shallower, which is well within the estimated uncertainty of 2 km. In any case, such a level of uncertainty is much lower than the factor 2-10 expected in the discrepancy between the geodetic and seismic moment estimates in the case of magma assisted opening and hence do not impact our conclusion ruling out magma intrusion (Biggs et al. 2010).

**7.4 Implication in terms of natural hazards assessment.**

Strain accommodation by magma intrusion functions to decrease the amount of extension accommodated by fault-slip in the volcanically active sectors of the eastern branch of the EAR (Parson and Thompson, 1991; Keir et al., 2006; Ebinger et al., 2008). This, combined with the thermal weakening of the lithosphere caused by higher rates of heat flow associated with magmatism (e.g. Ebinger and Hayward, 1996), and the ability of magma intrusion to accommodate extensional strain at lower stresses than brittle faulting (e.g. Rubin, 1992; Bialas et al., 2010), all function reduce the likelihood of large magnitude earthquakes in magma-rich extensional environments. For example the low-magnitude tectonic earthquakes recorded in the Virunga Volcanic Province (VVP) (generally ≤ Mw 4) contrast with stronger events recorded elsewhere in the Kivu basin (≤ Mw 6.2), and with major events recorded in the adjacent Albertine and Tanganyika basins (≤ Mw 7). In the less mature western branch, aside from volcanic provinces, most of the extension is accommodated through slip along the basins' border faults (Mavonga & Durrheim 2009; Albaric et al. 2009; Delvaux & Barth 2010).

The mode of extension in the South Kivu Volcanic Province (SKVP) is less well understood. Pre-rift volcanism started in the East Kivu basin with fissure eruptions of tholeiitic lavas in the mid-Miocene (10 – 7.5 Myr). The volcanism transitioned to alkali-basaltic lavas erupted in localized rifts during the opening of Lake Kivu (7.5-5 Myr). Volcanism ended approximately 175,000 years ago, with small volcanic eruptions close to the main active faults that bordered the rift valley to the west (Pasteels et al. 1989; Kampunzu et al. 1998; Furman & Graham 1999; Ebinger & Furman 2003/2003).

Even though volcanism initiated more recently in the SKVP than in the VVP, no active volcanoes are located in the SKVP, while Nyiragongo and Nyamuragira are still very active (Smets et al., 2010). The present finding that the Bukavu earthquake is not associated with magmatic activity favors a mode of rift opening in which crustal extension is accommodated seismically. If extension in the SKVP is mainly accommodated by fault slip, rather than via magmatic intrusions, this implies an increased risk for large, potentially destructive earthquakes in this region

Unfortunately, due to the insecurity in the region, detailed studies of structural geology and the collection of geodetic and seismic data is not currently possible. The remotely sensed topographic maps (SRTM – Farr et al. 2007) do not have sufficient resolution for in-depth geomorphologic studies, and optical imagery is affected by dense vegetation.

Hence we lack the data required to infer the locations and dimensions of faults that are needed to assess the seismic efficiency - the ratio between the observed and expected seismic moment – allowing an estimation of the fractions of extension accommodated seismically and aseismically (Hofstetter & Beyth 2003).

Finally, even if an in-depth discussion of the related risk in the Kivu basin is beyond the scope of the present paper, it is clear that the vulnerability of the Bukavu area remains high due to potential larger earthquakes in neighboring basins. For instance Mavonga & Durrheim (2009) estimates that the maximum earthquake magnitude expected for the Kivu basin is 6.7, and from his work, one can assess a return period of about 200 years. Such an assessment has important implications for related risks in this landslide-prone area (Moyersons et al. 2004) located on the shores of Lake Kivu, which contains high concentrations of dissolved carbon dioxide and methane (Schmid et al. 2005; Tassi et al. 2009). Unlike Lake Nyos and Lake Monoun in Cameroon (Kling et al. 1987), the waters of Lake Kivu are not yet saturated with these gases (Nayar 2009). However a mixing event caused by a large magma intrusion, landslide or earthquake could force overturn as has occurred in the past (Haberyan & Hecky 1987).

## 8. Conclusions

Independent inversions of seismic and two unrelated geodetic data sets, supplemented with local field and seismic observations, have established that the Bukavu earthquake occurred under southern Lake Kivu at a shallow depth of 9 km. Modeling suggests that this earthquake occurred on a normal fault striking N-S and dipping 50-60° eastward consistent with geophysical and geological observations in the area, although a shallow-dipping fault plane cannot be ruled out from the analysis of our data.

The good agreement between results derived from seismic and geodetic data illustrates that earthquake source parameters can be accurately estimated from InSAR, even in the case of a moderate-sized earthquake in a vegetated area.

The similarity between the geodetic and the seismic moments suggests that the observed deformation is almost entirely coseismic and related to a brittle rupture, which leads us to discard the hypothesis of magma involvement at shallow depth.

The present results are especially important for the assessment of the long-term style of extension along that portion of the rift and the related hazards. This study also shows the importance of carrying out systematic monitoring of the East African Rift using InSAR, as well as maintaining an archive of acquired images. In addition, it is imperative that the local seismic network be improved so that seismic risk can be better quantified.

## 9. Acknowledgments

SAR data were provided in the frame of European Space Agency (ESA) Cat-1 project nr 3224 and ESA-JAXA ALOS-ADEN AO project nr 3690. Precise orbits are provided by the Delft Institute of Earth Observation and Space Systems (DEOS) and ESA. Interferograms are computed with DORIS (TU Delft) (Kampes et al. 2003) and ROI-PAC (Caltech/JPL) (Rosen et al., 2004) software. Seismic data were provided by the Global Seismographic Network and the “SEARIFT” (NSF funded Afar project) and Afar Consortium seismic arrays in Ethiopia (NERC funded Afar project). We thank the whole staff of the Goma Volcano Observatory, which accomplishes its tasks in a difficult political and economic context. Benoit Smets digitized the geological map of Villeneuve (1980). Maps were prepared using the Generic Mapping Tool (Wessel & Smith 1998). This work is supported by the Belgian Science Policy under projects SAMAAV and GORISK (SR/00/113), and the National Research Fund of Luxembourg under the project FNR/STEREOII/06/01. Research by AS was supported by a NSF Graduate Research Fellowship. Research by PJG and JF was supported by project CGL2005-05500-C02 and carried out in the frame of the Moncloa Campus of International Excellence (UCM-UPM, CSIC). We thank Derek Keir and an anonymous reviewer whose comments helped to improve the manuscript.



## 10. References

Albaric, J., Déverchère, J., Petit, C., Perrot, J. & Le Gall, B., 2009. Crustal rheology and depth distribution of earthquakes: Insights from the central and southern East African Rift System, *Tectonophysics*, **468**, 28-41

Amelung, F. & Bell, J. W., 2003. Interferometric synthetic aperture radar observations of the 1994 Double Spring Flat, Nevada, earthquake (M5.9): Main shock accompanied by triggered slip on a conjugate fault, *J. Geophys. Res.,* ***108***(B9), 2433, doi:10.1029/2002JB001953.

Arvidsson, R. & Ekström, G., 1998. Global CMT analysis of moderate earthquakes, Mw≥4.5, using intermediate-period surface waves, *Bull. Seism. Soc. Am.*, ***88*** (4): 1003-1013.

Ayele, A., Keir, D., Ebinger, C., Wright, T. J., Stuart, G. W., Buck, W. R., Jacques, E., Ogubazghi, G. & Sholan, J., 2009. The September 2005 mega-dike emplacement in the Manda-Hararo (Afar) nascent oceanic rift, *Geophys. Res. Lett.*, **36**, 20306, doi:10.1029/2009GL039605.

Baer, G. & and Hamiel Y., 2010. Form and growth of an embryonic continental rift: InSAR observations and modelling of the 2009 western Arabia rifting episode. *Geophys. J. Int.*, **182**, 155-167, doi: 10.1111/j.1365-246X.2010.04627.x

Barth, A., Wenzel, F. & Giardini, D., 2007. Frequency sensitive moment tensor inversion for light to moderate magnitude earthquakes in eastern Africa, *Geophys. Res. Lett.*, **34**, 15302, doi:10.1029/2007GL030359.

Bialas, R., Buck, R. & Qin, R., 2010. How much magma is required to rift a continent? *Earth and Planetary Science Letters*, **292**, 68-78, doi:10.1016/j.epsl.2010.01.021

Biggs, J., Robinson, D. P. & Dixon, T. H., 2009a. The 2007 Pisco, Peru, earthquake (M8.0): seismology and geodesy. *Geophys. J. Int.,* ***176***, 657–669 doi: 10.1111/j.1365-246X.2008.03990.x.

Biggs J., Amelung, F., Gourmelen, N., Dixon, T. H. & Kim, S.-W., 2009b. InSAR observations of 2007 Tanzania rifting episode reveal mixed fault and dyke extension in an immature continental rift. *Geophys. J. Int.,* ***179***, 549–558, doi: 10.1111/j.1365-246X.2009.04262.x.

Biggs, J., Nissen, E., Craig, T., Jackson, J. & Robinson, D. P., 2010. Breaking up the hanging wall of a rift-border fault: The 2009 Karonga earthquakes, Malawi. *Geophys. Res. Lett.*, **37**, 11305, doi:10.1029/2010GL043179.

Bonjer, K.P., Fucha, K. & Wohlenberg, J., 1970. Crustal structure of the East African Rift system for spectral response ratios of long-period body waves, *Zeitshr. Geophys.*, ***36***: 287-297 .

Bonaccorso, A., Cianetti, S., Giunchi, C., Trasatti, E., Bonafede, M. & Boschi, E., 2005. Analytical and 3-D numerical modelling of Mt. Etna (Italy) volcano inflation. *Geophys. J. Int.*, **163**, 852-862.

Bram, K., 1975. Zum Aufbau der Kruste und oberen mantels in bereich des weslichen grabens des Ostrafrikansichen Grabensystem und im Ostlinchen Zaire-Bechen, Ergebnisse Einer Untersuchung der Raumwellem von Nah-Erdbeben, *Geophysikalische Abhandlungen*, ***4***, Institut fur Geophysik, Freie Universitat, Berlin, 1–65.

Buck, R., 1988. Flexural rotation of normal faults, *Tectonics, 7*(5), 959-973.

Bürgmann R., Rosen, P. A. & Fielding, E. J., 2000. Synthetic aperture radar interferometry to measure Earth's surface topography and its deformation, *Annu. Rev. Earth Planet. Sci.,* **28**:169–209.

Calais, E. , d'Oreye, N., Albaric, J. , Deschamps, A., Delvaux, D., Déverchère, J., Ebinger, C., Ferdinand, R. W. ,Kervyn, F., Macheyeki, A. S., Oyen, A., Perrot, J., Saria, E., Smets, B., Stamps, D. S. & Wauthier, C., 2008. Aseismic strain accommodation by slow slip and dyking in a youthful continental rift, East Africa, *Nature,* ***456***(7223), 783-788, doi:10.1038/nature07478.

Cattin, R., Briole, P., Lyon-Caen, H., Bernard, P. & Pinettes, P., 1999. Effects of superficial layers on coseismic displacements for a dip-slip fault and geophysical implications. *Geophys. J. Int.,* **137,** 149-158.

Chen, C.W. & Zebker, H.A., 2001. Two-dimensional phase unwrapping with use of statistical models for cost functions in nonlinear optimization, *Journal of the Optical Society of America, A,* ***18***, 338-351.

Dawson J., & Tregoning, P., 2007. Uncertainty analysis of earthquake source parameters determined from InSAR: A simulation study, *J. Geophys. Res.*, ***112***, 09406, doi:10.1029/2007JB005209.

Dawson, J., Cummins, P., Tregoning, P. & Leonard, M., 2008. Shallow intraplate earthquakes in Western Australia observed by Interferometric Synthetic Aperture Radar, *J. Geophys. Res.,* ***113***, 11408, Doi:10.1029/2008JB005807.

Delvaux, D. & Barth, A., 2010. African stress pattern from formal inversion of focal mechanism data, *Tectonophysics*, **482**, 105-128.

d'Oreye N., Kervyn, F., Calais, E., Cayol, V., Fernández, J., Frischknecht, C. , González, P.J., Heleno, S., Oyen, A. & Wauthier, C., 2008. Systematic InSAR Monitoring of African Active Volcanic Zones: What we have learned in three years, or a harvest beyond our expectations, *Proc. Second workshop on USE of Remote Sensing Techniques for Monitoring Volcanoes and Seismogenic Areas (USEReST 2008)*, Naples, Italy, 1-4244-2547-1/08/$20.00 ©2008 IEEE, 57-62.

Dubois L., Feigl, K.L., Komatitsch, D., Árnadóttir, T. & Sigmundsson, F., 2008. Three-dimensional mechanical models for the June 2000 earthquake sequence in the south Iceland seismic zone. *Tectonophysics*, **457**(1-2), 12-29.

Dziewonski, A.M. & Anderson, D.L., 1981. Preliminary Reference Earth Model (PREM), *Phys. Earth Planet. In.,* ***25***, 297-356.

Dziewonski, A.M., Chou, T.-A. & Woodhouse, J.H., 1981. Determination of earthquake source parameters from waveform data for studies of global and regional seismicity, *J. Geophys. Res.*, ***86*** (B4), 2825-2852.

Ebinger, C. J., 1989. Geometric and Kinematic development of border faults and accommodation zones, Kivu-Rusizi Rift, Africa, *Tectonics*, ***8***(1), 117–133.

Ebinger, C. J., Deino, A. L., Drake, R. E., & Tesha, A. L., 1989. Chronology of Volcanism and Rift Basin Propagation: Rungwe Volcanic Province, East Africa, *J. Geophys. Res.*, ***94***(B11), 15,785–15,803.

Ebinger, C. J., Karner, G. D. & Weissel, J. K., 1991. Mechanical strength of extended continental lithosphere: constraints from the Western Rift System, East Africa. *Tectonics,* ***10(***6), 1239-1256.

Ebinger C. J. & Hayward, N., 1996. Soft plates and hot spots: Views from Afar, *J. Geophys. Res.*,**101(B10)**, 21,859-21,876.

Ebinger, C. & Furman, T., 2002/2003. Geodynamical setting of the Virunga volcanic province, East Africa. *Acta Vulcanologica*, **14/15**(1-2), 9-16.

Ebinger, C.J., Keir, D., Ayele, A., Calais, E., Wright, T. J., Belachew, M., Hammond, J. O. S., Campbell, E. & Buck, W. R., 2008. Capturing magma intrusion and faulting processes during continental rupture: seismicity of the Dabbahu (Afar) rift. *Geophys. J. Int.,* **174**, 1138-1152.

Ebinger, C., Ayele, A., Keir, D., Rowland, J., Yirgu, G., Wright, T., Belachew, M. & Hamling, I., 2010. Length and timescales of rift faulting and magma intrusion: the Afar rifting cycle from 2005 to present, *Annu. Rev. Earth Planet. Sci.,* **38**, 437-464, doi:10.1146/annurev-earth-040809-152333.

Ekström, G., 1989. A very broad band inversion method for the recovery of earthquake source parameters". *Tectonophysics*, ***166***: 73-100.

Farr, T.G., Rosen, P.A., Caro, E., Crippen, R., Duren, R., 2007. The Shuttle Radar Topography Mission, *Rev. of Geophys.,* ***45***, RG2004, doi:10.1029 /2005RG000183.

Feigl, K., Geasperi, J., Sigmundsson, F. & Rigo, A., 2000. Crustal deformation near Hengill volcano, Iceland 1993-1998: Coupling between magmatic activity and faulting inferred from elastic modeling of satellite radar interferograms. *J. Geophys. Res.*, **105**, 25655-25670.

Feigl, K. L. & Thurber, C. H., 2009. A method for modelling radar interferograms without phase unwrapping: application to the M 5 Fawnskin, California earthquake of 1992 December 4, *Geophys. J. Int.,* ***176***, 491–504, doi: 10.1111/j.1365-246X.2008.03881.x.

Foster, A.N. & Jackson, J.A., 1998. Source parameters of large African earthquakes:implications for crustal rheology and regional kinematics. *Geophys. J. Int.*, **134**, 422-448.

Furman, T. & Graham, D., 1999. Erosion of lithospheric mantle beneath the East African Rift system: geochemical evidence from the Kivu volcanic province. *Lithos,* **48,** 237-262.

Grandin, R., Socquet, A., Binet, R., Klinger, Y., Jacques, E., de Chabalier, J.-B., King, G. C. P., Lasserre, C., Tait, S., Tapponnier, P., Delorme, A. & Pinzuti, P., 2009. September 2005 Manda Hararo-Dabbahu rifting event, Afar (Ethiopia): Constraints provided by geodetic data, *J. Geophys. Res.,* **114**, B08404, doi:10.1029/2008JB005843.

Haberyan, K.A. & Hecky, R.E., 1987. The late Pleistocene and Holocene stratigraphy and paleolimnology of Lakes Kivu and Tanganyika. *Palaeogeography, Palaeoclimatology, Palaeoecology,* **61**, 169-197.

Hamaguchi, H., Nishimura, T. & Zana, N., 1992. Process of the 1977 Nyiragongo eruption inferred from the analysis of long-period earthquakes and volcanic tremors, *Tectonophysics, **209**,* 241-254

Hamling, I. J., Ayele, A., Bennati, L., Calais, E., Ebinger, C. J., Keir, D., Lewi, E., Wright, T. J. & Yirgu, G., 2009. Geodetic observations of the ongoing Dabbahu rifting episode: new dyke intrusions in 2006 and 2007, *Geophys. J. Int., **178***, 989–1003, doi: 10.1111/j.1365-246X.2009.04163.x.

He, Y-M., Wang, W-M. & Yao, Z-X., 2003. Static Deformation Due to Shear and Tensile Faults in a Layered Half-Space. *Bull. Seism. Soc. Am.*, **93**, 2253-2263.

Hofstetter, R. & Beyth, M., 2003. The Afar Depression: interpretation of the 1960-2000 earthquakes. *Geophys. J. Int.,* **155**, 715-732.

Kampes B., Hanssen, R. & Perski, Z., 2003. Radar interferometry with public domain tools, *Proceedings of the 2nd ESA Fringe2003 workshop*, ESA-ESRIN, Frascati, Italy.

Kampunzu, A. B., Bonhomme, M. G. & Kanika, M., 1998. Geochronology of volcanic rocks and evolution of the Cenozoic Western Branch of the East African rift system. *Journal of African Earth Sciences*, **26**, 441-461.

Kavotha, S.K., Mavonga, T., Durieux, J. & Mukambilwa, K., 2002/2003. Towards a more detailed seismic picture of the January 17th, 2002 Nyiragongo Eruption, *Acta Vulcanologica*, ***14/15*** (1-2): 87-100.

Kasahara, M. , Hamaguchi, H., Tanaka, K., Zana, N. & Kabwik, M., 1992. Recent horizontal crustal movements in and around volcano Nyamuragira, Zaire, *Tectonophysics,* **209**, 267-272.

Keir, D., Ebinger, C. J., Stuart, G. W., Daly, E. & Ayele, A., 2006. Strain accommodation by magmatism and faulting as rifting proceeds to breakup: Seismicity of the northern Ethiopian rift. *J. Geophys. Res.*, **111**, 05314, doi:10.1029/2005JB003748.

Keir D., Hamling, I. J., Ayele, A., Calais, E., Ebinger, C., Wright, T. J., Jacques, E., Mohamed, K., Hammond, J. O.S., Belachew, M., Baker, E., Rowland, J. V., Lewi, E. & Bennati, L., 2009. Evidence for focused magmatic accretion at segment centers from lateral dike injections captured beneath the Red Sea rift in Afar, *Geology*, **37**, 59-62.

Kling, G.W. et al., 1987. The 1986 Lake Nyos Gas Disaster in Cameroon, West Africa, *Science*,**236**, 169-175.

Komorowski J.C. et al., 2002/2003. The January 2002 eruption - The January 2002 flank eruption of Nyiragongo Volcano (Democratic Republic of Congo): chronology, evidence for a tectonic rift trigger, and impact of lava flows on the city of Goma, *Acta Vulcanologica, **14/15(***1-2), 27-62, doi: 10.1400/19087.

Kontoes, C., Elias, P., Sykioti, O., Briole, P., Remy, D., Sachpazi, M., Veis, G. & Kotsis, I., 2000. Displacement field and fault model for the September 7, 1999 Athens earthquake inferred from ERS2 satellite radar interferometry, *Geophys. Res. Lett.*, **27**(24), 3989-3992.

Lerch, D.W., Klemperer, S.L., Egger, A.E., Colgan, J.P. & Miller, E.L., 2010. The northwestern margin of the Basin-and-Range Province, part 1: Reflection profiling of the moderate-angle (~ 30°) Surprise Valley Fault. *Tectonophysics*, **488,** 143-149.

Lohman R.B., Simons, M. & Savage, B., 2002. Location and mechanism of the Little Skull Mountain earthquake as constrained by satellite radar interferometry and seismic waveform modeling, *J. Geophys. Res.*, ***107***(B6), 2118, 10.1029/2001JB000627

Lohman, R.B. & Simons, M., 2005. Locations of selected small earthquakes in the Zagros mountains. *Geochem. Geophys. Geosys.*, ***6***(1), Q03001, doi:10.1029/2004GC000849

Lomax, A., Virieux, J., Volant, P. & Berge, C., 2000. Probabilistic earthquake location in 3D and layered models: Introduction of a Metropolis-Gibbs method and comparison with linear locations. *Advances in Seismic Event Location,* Thurber, C.H., and N. Rabinowitz (eds.), Kluwer, Amsterdam, 101-134.

Massonnet, D. & Feigl, K., 1998. Radar interferometry and its application to changes in the Earth's surface. *Rev. Geophys.,* ***36*** (4), 441-500.

Masterlark, T. & Hughes,K.L.H., 2008. Next generation of deformation models for the 2004 M9 Sumatra-Andaman earthquake. *Geophys. Res. Lett.* **35**(19), 19310, doi:10.1029/2008GL035198.

Mavonga, T., Kavotha, S.K., Lukaya, N., Etoy O. and Durieux, J., 2006. Seismic activity prior to the May 8, 2004 eruption of volcano Nyamuragira, Western Rift Valley of Africa. *Journal of Volcanology and Geothermal Research.* **158**, 355-360.

Mavonga, T., 2007. Some characteristics of aftershock sequences of major earthquakes from 1994 to 2002 in the Kivu province, Western Rift Valley of Africa, *Tectonophysics*, **439**, 1-12.

Mavonga, T. & Durrheim, R.J., 2009. Probabilistic seismic hazard assessment for the Democratic Republic of Congo and surrounding areas. *South African Journal of Geology,* **112**, 329-342.

Mellors R.J., Magistrale, H., Earle, P. & Cogbill, A., 2004. Comparison of Four Moderate-Size Earthquakes in Southern California Using Seismology and InSAR, *Bull. Seism. Soc. Am., **94**(6)*, 2004–2014.

Moeyersons, J., Tréfois, P., Lavreau, J., Alimasi, D., Badriyo, I., Mitima, B., Mundala, M., Munganga, D.O. & Nahimana, L., 2004. A geomorphological assessment of landslide origin at Bukavu, Democratic Republic of the Congo. *Engineering Geology,* **72**(1-2), 73-87.

Montgomery-Brown, E.K., . Segall,P. & Miklius, A., 2009. Kilauea slow slip events: Identification, source inversions, and relation to seismicity. *J. Geophys. Res.*, **114,** 00A03, doi:10.1029/2008JB006074.

Morley, C. K., 1989. Extension, detachments, and sedimentation in continental rifts (with particular reference to East Africa), *Tectonics*, ***8***(6), 1175–1192.

Morley, C. K., 2002. Tectonic settings of continental extensional provinces and their impact on sedimentation and hydrocarbon prospectivity. *Sedimentation in Continental Rifts, SPECIAL PUBLICATION-SEPM*, **73,** 25-55.

Nayar, A., 2009. Earth science: A lakeful of trouble. *Nature,* **460**(7253), 321-323.

Nelder, J.A. and Mead, R., 1965. A simplex method for function minimization, *The Computer Journal,* **7***,* 308-313; doi:10.1093/comjnl/7.4.308

OCHA, Regional Office for Central Africa and East Africa, 2008. Earthquake in the Great Lakes Regions, *Regional situation update report,* 15 February 2008.

Okada, Y., 1985. Surface deformation due to shear and tensile faults in a half-space, *Bull. Seism. Soc. Am.*, **75**, 1135-1154.

Pagli C., Sigmundsson, F., Pedersen, R., Einarsson, P., Arnadottir, T. & Feigl, K. L., 2007. Crustal deformation associated with the 1996 Gjalp subglacial eruption, Iceland: InSAR studies in affected areas adjacent to the Vatnajokull ice cap, *Earth Planet. Sci. Lett.*, **259**, 24-33, DOI: 10.1016/j.epsl.2007.04.019.

Pallister, J.S. et al., 2010. Broad accommodation of rift-related extension recorded by dyke intrusion in Saudi Arabia. *Nature Geoscience,* **3**, 705-712, doi: 10.1038/ngeo966

Parsons, T. & Thompson, G.A., 1991. The Role of Magma Overpressure in Suppressing Earthquakes and Topography: Worldwide Examples. *Science,* **253**, 1399-1402.

Pasteels, P., Villeneuve, M., De Paepe, P. & Klerkx, J., 1989. Timing of the volcanism of the southern Kivu province: implications for the evolution of the western branch of the East African Rift system. *Earth Planet. Sci. Lett.*,**94,** 353-363.

Pérez-Gussinyé, M., Metois, M., Fernández, M., Vergés, J., Fullea, J. & Lowry, A.R., 2009. Effective elastic thickness of Africa and its relationship to other proxies for lithospheric structure and surface tectonics. *Earth Planet. Sci. Lett.*, **287**, 152-167

Pritchard, M. E. & Fielding, E. J., 2008. A study of the 2006 and 2007 earthquake sequence of Pisco, Peru, with InSAR and teleseismic data. *Geophys. Res. Let., **35***, 09308, doi:10.1029/2008GL033374.

Rigo, A. & Massonnet, D., 1999. Investigating the 1996 Pyrenean earthquake (France) with SAR Interferograms heavily distorted by atmosphere. *Geophys. Res. Lett.*, **26**(21), 3217-3220.

Rosen, P. A., Henley, S., Peltzer, G. & Simons M., 2004. Updated Repeat Orbit Interferometry Package Released, *Eos Trans. AGU*, **85**(5), 47.

Rubin, A., 1992. Dike-induced faulting and graben subsidence in volcanic rift zones. *J. Geophys. Res,* **97**(B2), 1839-1858.

Schmid, M. Halbwachs, M., Wehrli, B. & Wüest, A., 2005. Weak mixing in Lake Kivu: New insights indicate increasing risk of uncontrolled gas eruption. *Geochem. Geophys. Geosys.* **6**(7), 07009, doi:10.1029/2004GC000892.

Smets, B., Wauthier, C. & d'Oreye, N., 2010. A new map of the lava flow field of Nyamulagira (D.R.Congo) from satellite imagery. *Journal of African Earth Sciences,* In press.

Smith, G. & Ekström, G., 1996. Improving teleseismic event locations using a three dimensional Earth model. *Bull. Seismol. Soc. Am.* **86** (3), 788–796.

Stamps, D. S., Calais, E., Saria, E., Hartnady, C., Nocquet, J.-M., Ebinger, C. J. & Fernandes, R. M., 2008. A kinematic model for the East African Rift, *Geophys. Res. Lett.*, ***35***, L05304, doi:10.1029/2007GL032781.

Stramondo, S., Tesauro, M., Briole, P., Sansosti, E., Salvi, S., Lanari, R., Anzidei, M., Baldi, P., Fornaro, G., Avallone, A., Buongiorno, M.F., Franceschetti, G. & Boschi, E., 1999. The September 26, 1997 Colfiorito, Italy, earthquakes: modeled coseismic surface displacement from SAR interferometry and GPS, *Geophys. Res. Lett.*, **26**(7), 883-886.

Tassi, F., Vaselli, O., Tedesco, D., Montegrossi, G., Darrah, T., Cuoco, E., Mapendano, M. Y., Poreda, R. & Delgado Huertas, A., 2009. Water and gas chemistry at Lake Kivu (DRC): Geochemical evidence of vertical and horizontal heterogeneities in a multibasin structure. *Geochem. Geophys. Geosys.,* **10**(2), 02005, doi:10.1029/2008GC002191.

Tedesco, D., Vaselli, O., Papale, P., Carn, S. A., Voltaggio, M., Sawyer, G. M., Durieux, J., Kasereka, M. & Tassi, F., 2007. January 2002 volcano-tectonic eruption of Nyiragongo volcano, Democratic Republic of Congo, *J. Geophys. Res.*, ***112***, 09202, doi:10.1029/2006JB004762.

Tessema, A. & Antoine, L.A.G., 2003. Variation in effective elastic plate thickness of the East Africa lithosphere, *J. Geophys. Res.*, **108**, 2224, doi:10.1029/2002JB002200.

Utsu, T., 1961. A statistical study on the occurrence of aftershocks, *Geophys. Mag.,* ***30***, 521-605.

Villeneuve, M., 1980. La structure du Rift Africain dans la Région du Lac Kivu (Zaïre oriental), *B. Volcanol., **43**-3*, 541-551, DOI - 10.1007/BF02597691.

Wauthier, C., Cayol, V., Kervyn, F. & d'Oreye, N., In prep. Nyiragongo volcano 2002 eruption constrained by multibeam InSAR data.

Wessel, P. & Smith, W.H.F., 1998. New, improved version of the Generic Mapping Tools released, *EOS Trans. AGU* ***79***, 579.

Wright, T. J., Ebinger, C., Biggs, J., Ayele, A., Yirgu, G., Keir, D. & Stork, A., 2006. Magma-maintained rift segmentation at continental rupture in the 2005 Afar dyking episode, *Nature,* ***442***, 291 – 294.

## Figure legends

Figure 1 : Tectonic Map of Lake Kivu basin. Inset displays the location of the Kivu Basin within Africa. Main figure: brown discontinuous line is the DRC-Rwanda political border. White squares and dots marks mains cities or places mentioned in the text : Go, BK and CY are respectively Goma, Bukavu and Cynagugu cities ; Bi is Birava village; Ib is Ibinja island, Nyo and Nya are Nyiragongo and Nyamulagira volcanoes. Faults traces after Villeneuve (1980) are not all confirmed by field investigations. VVP and SKVP are Virunga and South Kivu Volcanic Provinces (light green).

Figure 2: Seismicity of the Lake Kivu region as recorded in the USGS catalog (1973-2009). Histogram: The total number of events per year is shaded black. The number of events with magnitude 5 or greater are drawn in color. Map: Events with magnitudes less than 5 are drawn in black. Larger events are drawn in color, corresponding to the histogram on top. The size of the circle corresponds to the earthquake magnitude. Maroon triangles are Holocene volcanoes (Smithsonian Institution Global Volcanism Project) and dashed lines indicate political boundaries. Note: The increase in events with time is due to improvements in the seismic network and detection techniques.

Figure 3: View of the landslide in Ibinja Island (located by the arrow in the inset). The ellipse encircles the top of banana trees now underwater. Viewing directions are marked on both side of the picture. The landslide rupture has replaced the previously gentle slope of the shoreline.

Figure 4: Local seismicity located by the temporary seismic network and the Goma Volcano Observatory seismic network from 8 – 30 February 2008. Among the 700 aftershocks detected by these networks, only 37 could be located with an estimated horizontal error (ERH) of less than 10 km (dark grey circles). Green and orange stars respectively show the location of the 2008 Bukavu-Cyangugu mainshock obtained from the geodetic inversion and the teleseismic data (this study). Inverted yellow triangles are the seismic stations; thin yellow lines are the political borders.

Figure 5. Focal mechanisms from the teleseismic data (this study) for the mainshock (2008/02/03 7:34:13), and for two aftershocks (northern is 2008/02/14 2:07:47, southern is 2008/02/03 10:56:10). Red dots show the National Earthquake Information Center's locations for earthquakes within a month of the mainshock. The green triangle shows the location of the rupture fault obtained from the geodetic inversion (this study).

Figure 6. Depth determination for the 2008 Bukavu-Cyangugu earthquake. Broadband teleseismic P and SH waveforms (solid) and calculated synthetic seismograms (dashed) are shown in the upper and lower panels respectively. Brackets across these curves show the time window being inverted and the arrows show the picked first arrivals. The station names and maximum amplitude (in microns) are printed for each waveform. The focal mechanism corresponding to the full moment tensor solution and the source time function determined by the inversion are also shown. The top focal mechanism shows both the non-double-couple and double-couple solutions from

broadband and CMT analysis. The shaded focal mechanism corresponds to the non-double-couple solution from broadband analysis.

Figure 7: Coseismic ground deformation (range displacement – positive away from the satellite, in cm) and models for uniform slip inversion for the 2008 Bukavu-Cyangugu earthquake. A): Unwrapped ascending track ALOS PALSAR interferogram spanning 29 December 2007 - 30 march 2008. D) Unwrapped descending track ENVISAT ASAR interferogram spanning 10 January – 14 February 2008 (see table 2 for details). Corresponding best-fit models of a uniform slip elastic dislocation are shown in B) and E). The black solid rectangle indicates the projection of the fault rupture onto the surface and the dashed line shows where the fault, if lengthened, would cut the surface. Residuals are shown in C) and F). Panels G) and H) zoom in the residuals around the fault area (ALOS and ENVISAT respectively) with a higher resolution color scale. Contour lines in each panel depict a 2.8cm range displacement.

Figure 8. Frequency histograms of the 9 parameters determined from 100 independent runs of the inversion algorithm. Histograms represent the 100 best-fit solution parameters (dark grey bins) obtained from joint inversions of ENVISAT and ALOS ground deformation maps. The optimal solution for the nine parameters is estimated from the mean value of the best-fit Gaussian (black curve). The starting parameters for each of the 100 inversions were chosen randomly within broad bounds: the depths of the top of the fault [2 – 10km], the latitude [2.3624°S – 2.4796°S], the longitude [28.9973°E – 28.8531°E], the amount of dip-slip [-0.25m – 2,5m] and strike-slip [-

0.2m – 0.2m], the dip [30° – 75°] and strike angles [-25° – 25°], and the width [5 – 15km] and length [5 – 15km] of the dislocation.

Figure 9. Matrix plot of the 100 best-fitting solutions for each of the 9 inverted source parameters of the 2008 Bukavu-Cyangugu earthquake estimated from ENVISAT and ALOS InSAR data.

## Tables

Table 1. Velocity model after (Bonjer et al., 1970) and (Bram, 1975)

| Thickness (km) | Vp (km/s) | Vs (km/s) |
|---|---|---|
| 0.0 | 4.0 | 2.31 |
| 3.0 | 6.0 | 3.46 |
| 20.0 | 6.7 | 3.87 |
| 30.0 | 7 | 4.04 |

Table 2: Parameters of the ENVISAT and ALOS radar data.

| **Satellite Wavelength** | **Orbit nrumber Date** | **Perp. baseline** | **Altitude of ambiguity** | **Look angle Mode** |
|---|---|---|---|---|
| ENVISAT ASAR C-band (5,6 cm) | 30650 - 31151 10 Jan. 2008 - 14 Feb. 2008 | 125 m | 82 m | 22° Desc. Orb. |
| ALOS PALSAR L-band (23,6 cm) | 10280 - 11622 29 Dec. 2007 - 30 Mar. 2008 | 111 m | 507 m | 34° Asc. Orb. |

Table 3: Source parameters (centroid) of the 2008 Bukavu-Cyangugu earthquake estimated from the seismic and geodetic inversions. Uncertainties (1 σ) given in the table are standard deviations; it is not meant as the accuracy. The accuracy of the epicenter location from the Broadband + CMT solution is typically an order of magnitude lower than ± 0,01 degree in Lat./Long uncertainty (i.e. of the order of a km). Similarly, assumptions about isotropy and rehology of the medium may also impact the source parameters accuracy up to few % (see § 7.3 for discussion).

| **Inversion data set** | **Depths (km)** | **Dip (Deg)** | **Strike (Deg)** | **Rake (Deg)** | **Latitude (Deg)** | **Longitude (Deg)** | **Moment ($10^{17}$ Nm)** |
|---|---|---|---|---|---|---|---|
| ENVISAT | 9.3 ± 0.6 | 46.6 ± 2.5 | 351.5 ± 10.0 | -91.5 ± 14.3 | 28.9425 ± 0.0009 | -2.4060 ± 0.0036 | 9.61 ± 0.10 |
| ALOS | 9.8 ± 0.3 | 63.0 ± 0.5 | 352.3 ± 0.5 | -92.5 ± 15.7 | 28.9196 ± 0.0006 | -2.4216 ± 0.0004 | 11.64 ± 0.02 |
| Joint ENVISAT+ALOS non-weighted | 8.9 ± 0.3 | 58.6 ± 0.8 | 352.4 ± 1.6 | -105.2 ± 16.6 | 28.9260 ± 0.0006 | -2.4219 ± 0.0020 | 9.79 ± 0.004 |
| Joint ENVISAT+ALOS weighted | 8.9 ± 0.4 | 55.1 ± 1.4 | 354.5 ± 1.4 | -97.9 ± 15.9 | 28.9299 ± 0.0850 | -2.4145 ± 0.369 | 8.99 ± 0.010 |
| Broadband+CMT | 7.8 ± 2.0 | 51.5 | 350.1 | -100.6 | 28.74 ± 0.01 | -2.45 ± 0.01 | 9.43 ± 0.06 |

# Figures

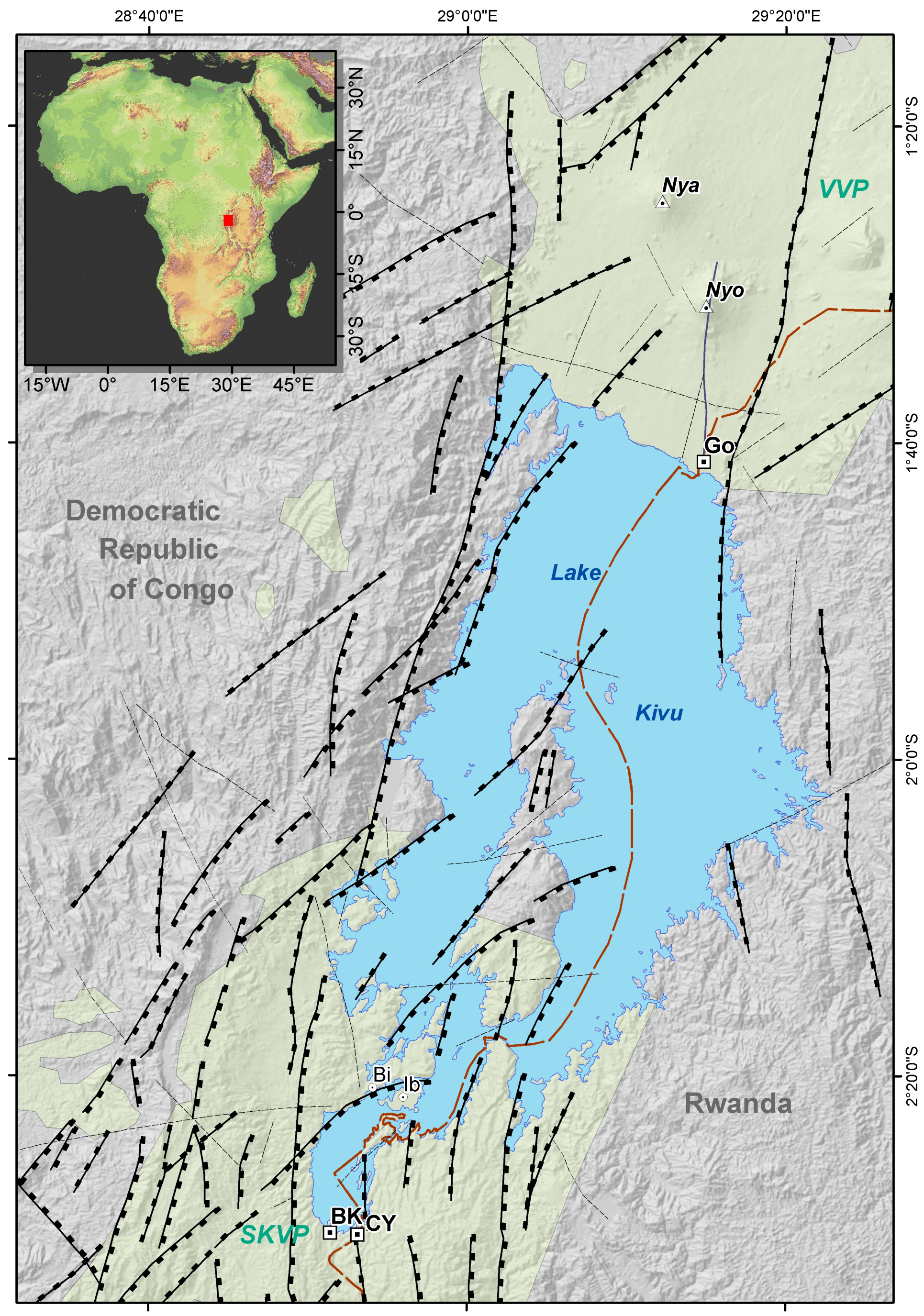


Figure 1.

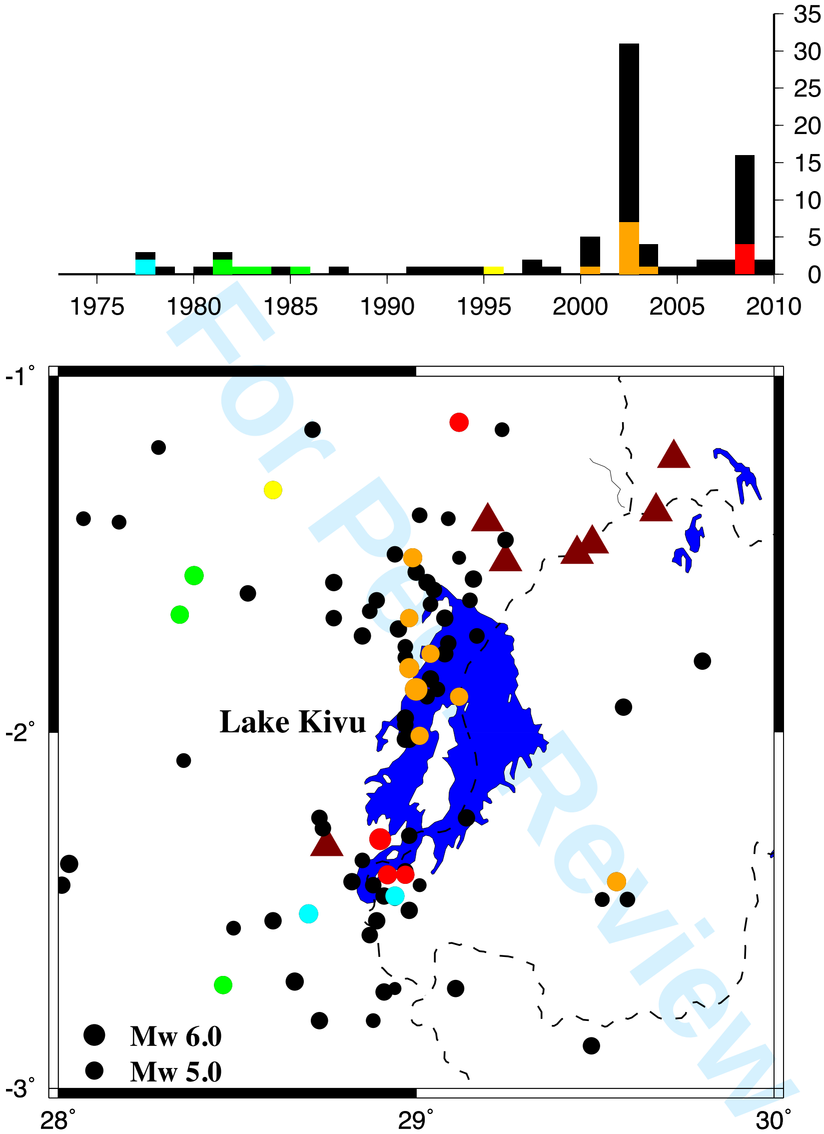
0
5
10
15
20
25
30
35
1975
1980
1985
1990
1995
2000
2005
2010
Lake Kivu
Mw 6.0
Mw 5.0
-1°
-2°
-3°
28°
29°
30°



**Figure 2.**

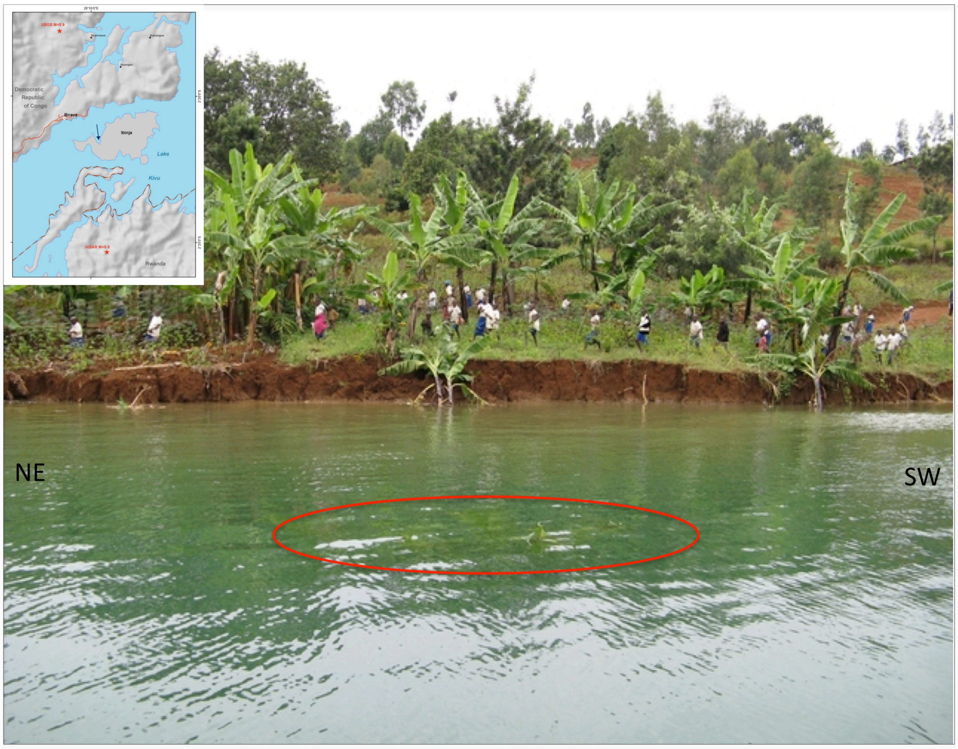
28°55'0"E
USGS M=5.9
Democratic
Republic
of Congo
Birava
Ibinja
Lake
Kivu
2°20'0"S
2°25'0"S
InSAR M=5.9
Rwanda
NE
SW

**Figure 3.**

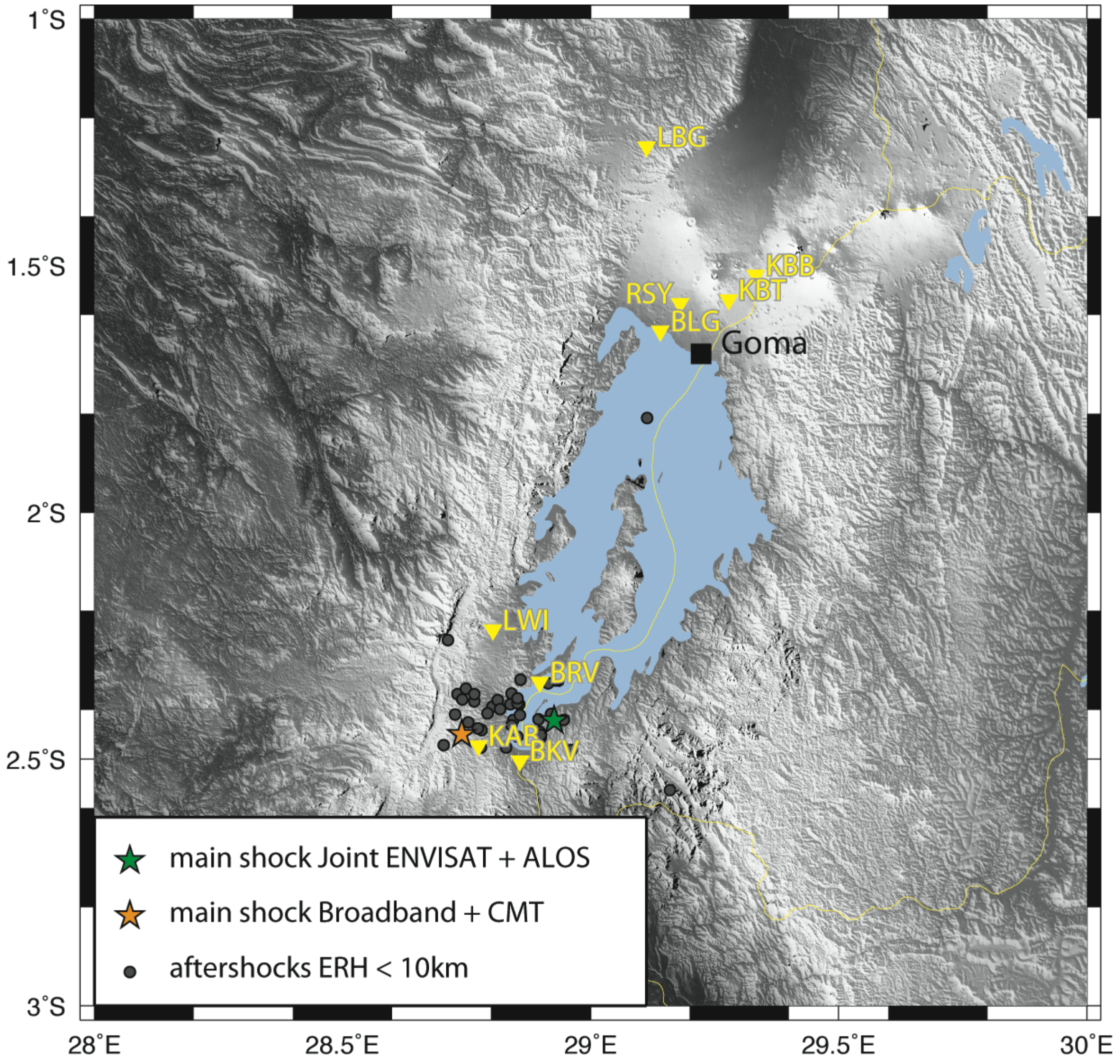


1059

1060 **Figure 4.**

1061

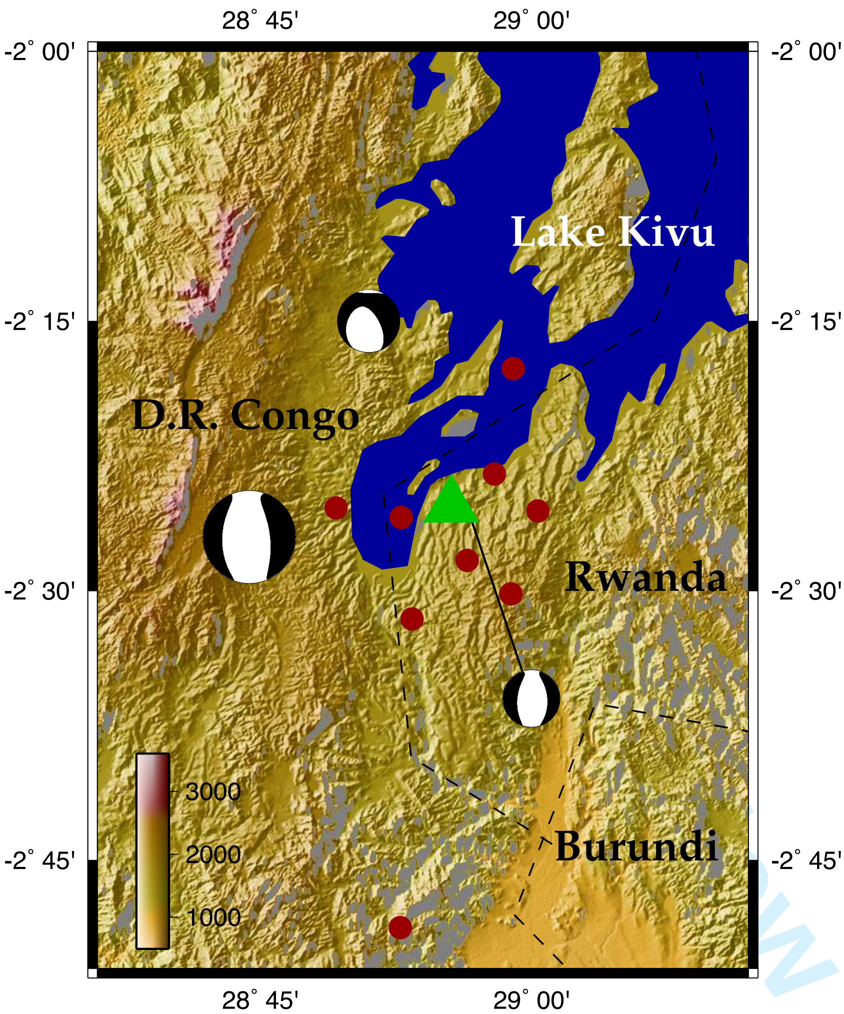
28° 45'
29° 00'
-2° 00'
-2° 15'
-2° 30'
-2° 45'
Lake Kivu
D.R. Congo
Rwanda
Burundi
3000
2000
1000

**Figure 5.**

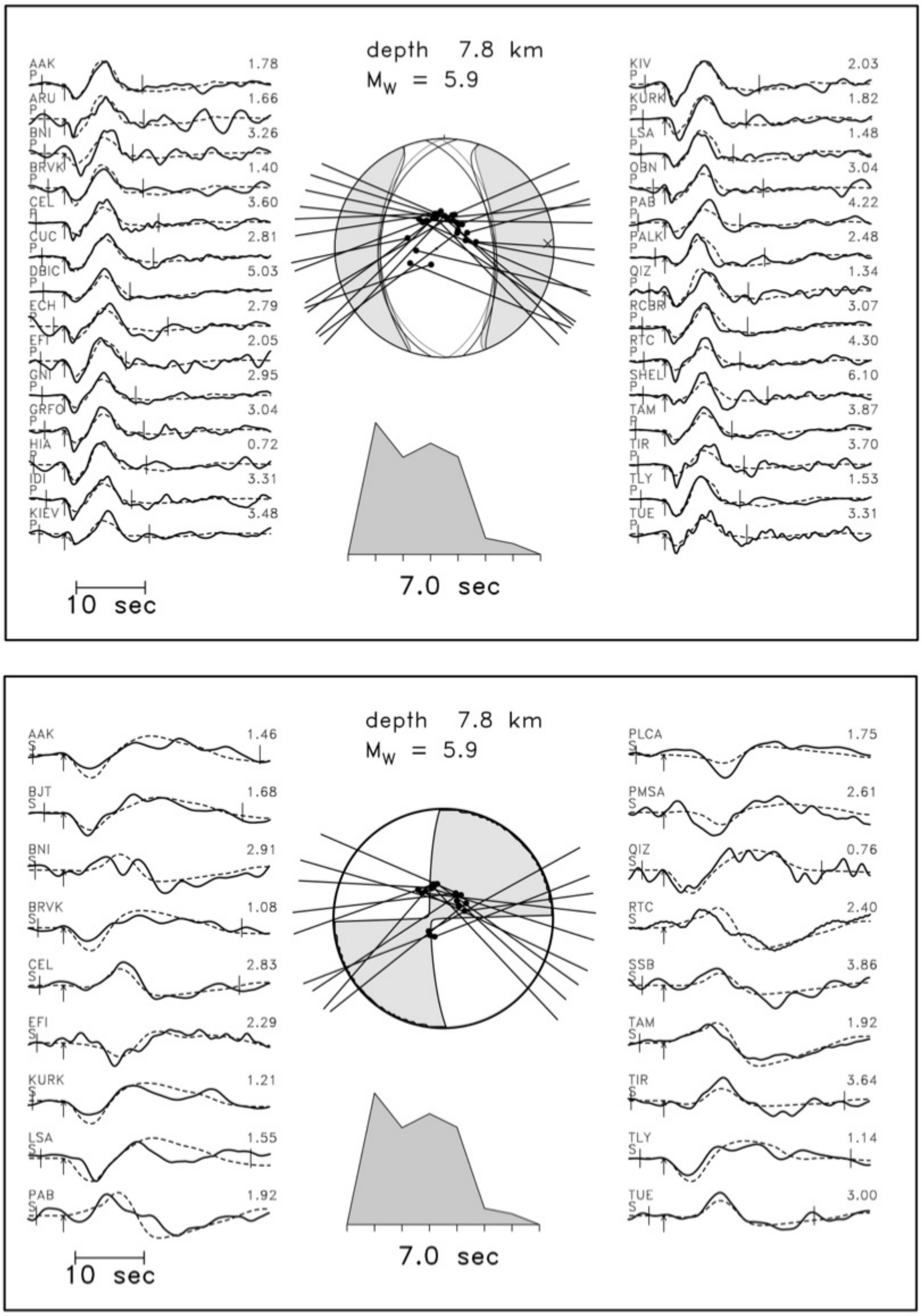
depth 7.8 km
$M_W$ = 5.9
AAK P 1.78
ARU P 1.66
BNI P 3.26
BRVK P 1.40
CEL P 3.60
CUC P 2.81
DBIC P 5.03
ECH P 2.79
EFI P 2.05
GNI P 2.95
GRFO P 3.04
HIA P 0.72
IDI P 3.31
KIEV P 3.48
KIV P 2.03
KURK P 1.82
LSA P 1.48
OBN P 3.04
PAB P 4.22
PALK P 2.48
QIZ P 1.34
RCBR P 3.07
RTC P 4.30
SHEL P 6.10
TAM P 3.87
TIR P 3.70
TLY P 1.53
TUE P 3.31
10 sec
7.0 sec
depth 7.8 km
$M_W$ = 5.9
AAK S 1.46
BJT S 1.68
BNI S 2.91
BRVK S 1.08
CEL S 2.83
EFI S 2.29
KURK S 1.21
LSA S 1.55
PAB S 1.92
PLCA S 1.75
PMSA S 2.61
QIZ S 0.76
RTC S 2.40
SSB S 3.86
TAM S 1.92
TIR S 3.64
TLY S 1.14
TUE S 3.00
10 sec
7.0 sec

**Figure 6.**

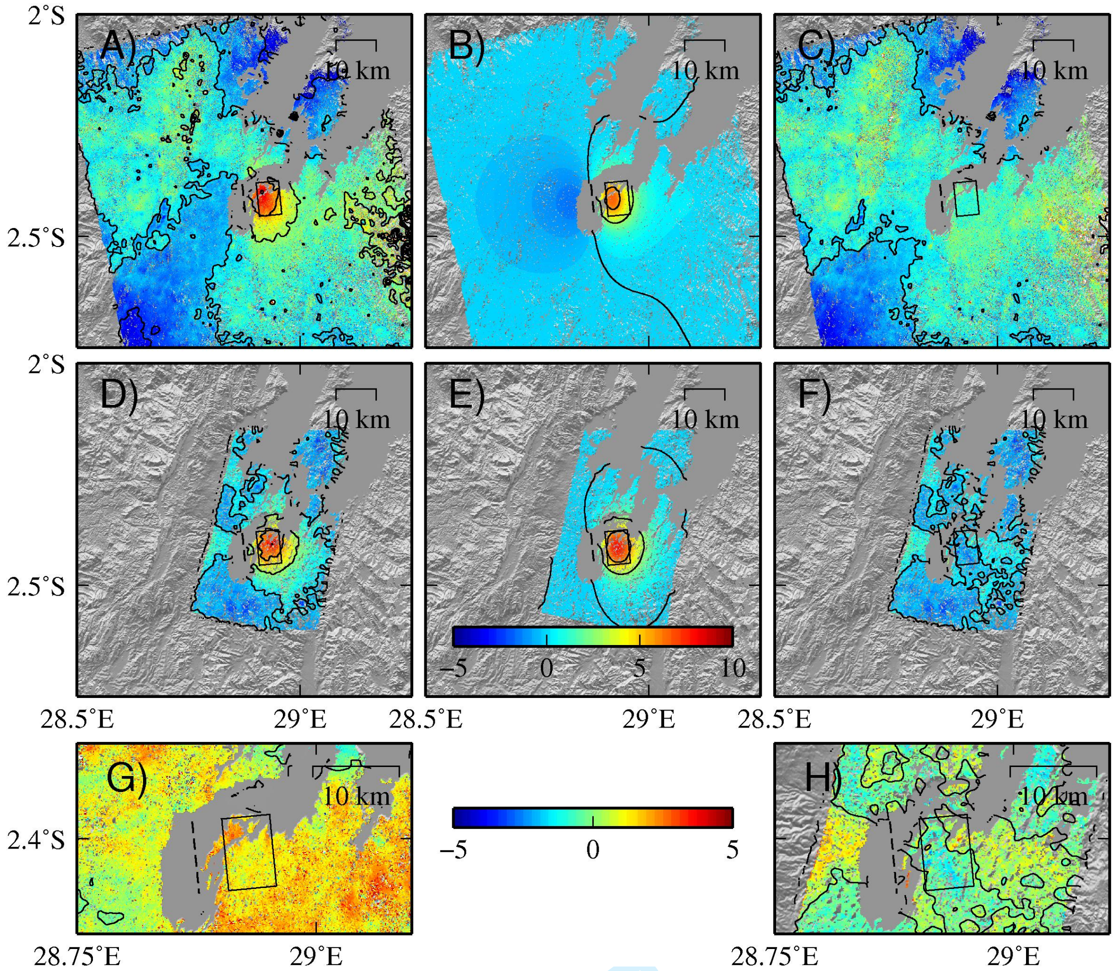


**Figure 7.**

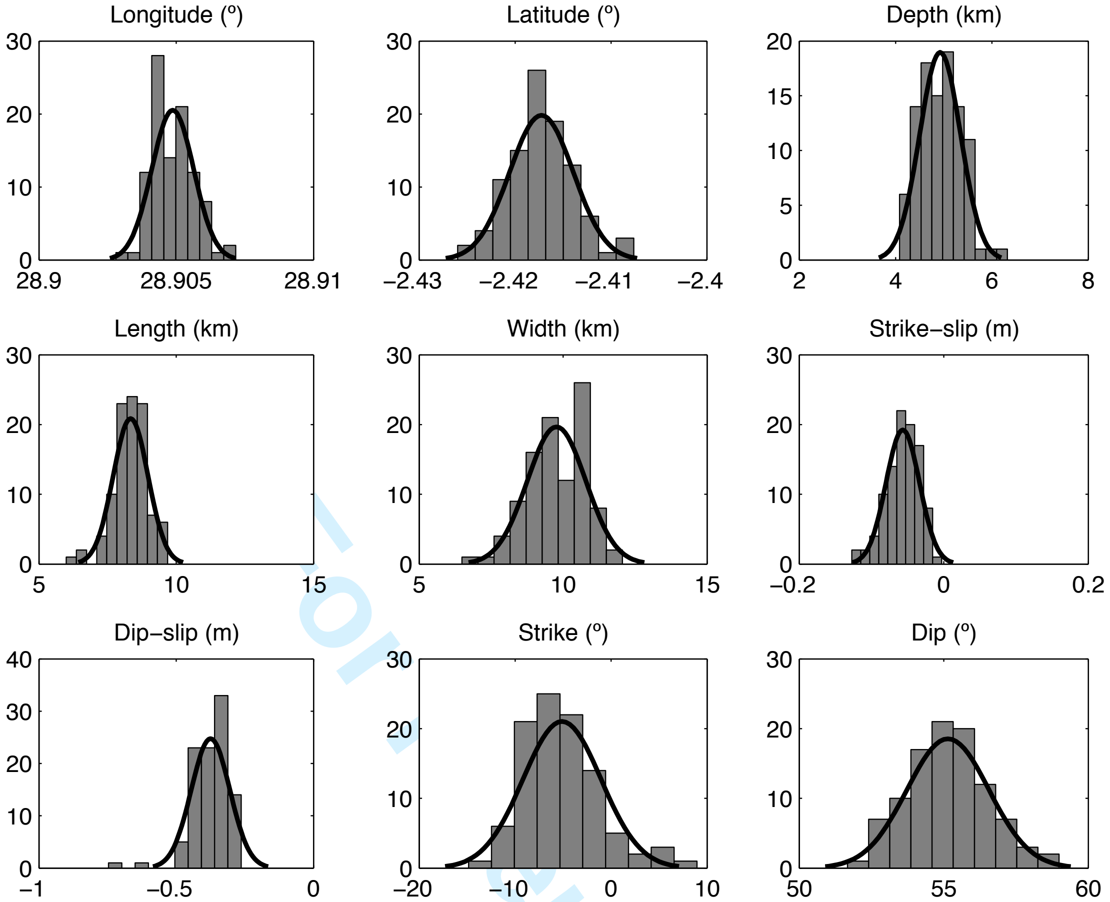
Longitude (º)
Latitude (º)
Depth (km)
Length (km)
Width (km)
Strike−slip (m)
Dip−slip (m)
Strike (º)
Dip (º)
28.9 28.905 28.91
−2.43 −2.42 −2.41 −2.4
2 4 6 8
5 10 15
−0.2 0 0.2
−1 −0.5 0
−20 −10 0 10
50 55 60

**Figure 8.**

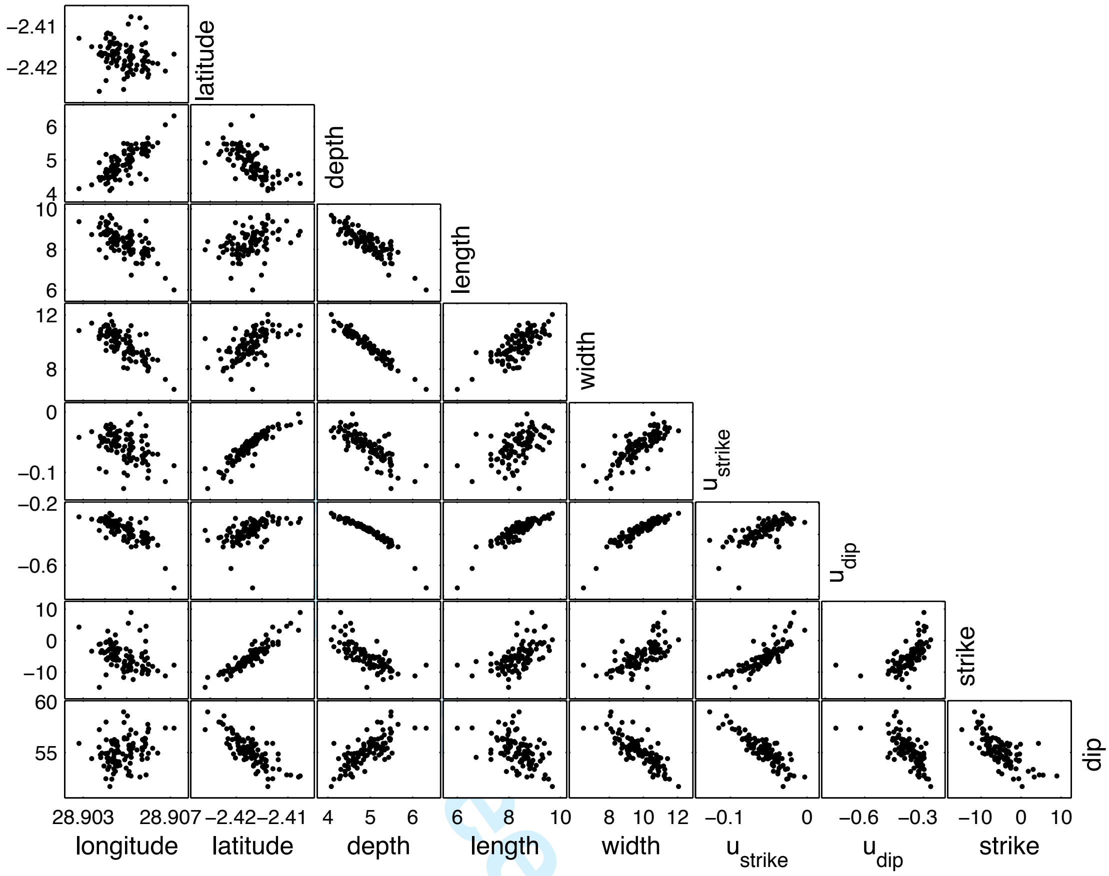
latitude
depth
length
width
$u_{strike}$
$u_{dip}$
strike
dip
−2.41
−2.42
6
5
4
10
8
6
12
8
0
−0.1
−0.2
−0.6
10
0
−10
60
55
28.903
28.907
longitude
−2.42
−2.41
latitude
4
5
6
depth
6
8
10
length
8
10
12
width
−0.1
0
$u_{strike}$
−0.6
−0.3
$u_{dip}$
−10
0
10
strike

**Figure 9.**